

# Viscous Flow Computation around the Wigley Hull with the Maneuvering Motion using the Inertial Coordinate System on the Non-inertial Grids

Yan Naing Win<sup>a\*</sup>, Yasuyuki Toda<sup>a</sup>

<sup>a</sup>Department of Naval Architecture and Ocean Engineering, Osaka University, Osaka, Japan 565-0871

\*Corresponding author: Yan\_Naing\_Win@naoe.eng.osaka-u.ac.jp

## Article history

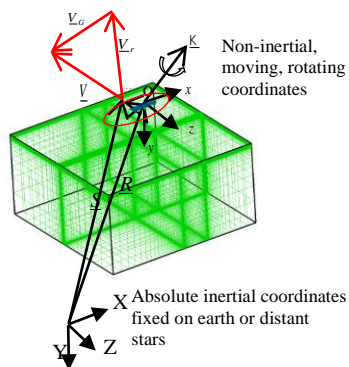
Received :27 July 2013

Received in revised form :

5 November 2013

Accepted :25 November 2013

## Graphical abstract



## Abstract

Computational Fluid Dynamics (CFD) technique for ship hydrodynamics has been well developed with advanced capabilities for resistance and propulsion, seakeeping, and maneuvering. The laboratory (Laboratory 3 of Department of Naval Architecture and Ocean Engineering in Osaka University) specializes in resistance and propulsion field and has carried out several simulations based on the CFD code in non-inertial ship-fixed coordinates system. The purpose of this research is to transform the present computation code to the one in inertial coordinate and to investigate the flow field around the Wigley hull for several motions up to three degrees of freedom (3 DOF). The transformed code is simulated on the flat plate initially and the nature of the flow field is investigated and confirmed with the hydrodynamics theory. Then, the wigley hull motions are simulated in several ways such as; uniform motion, pure yaw and circular motion test. The features of the flow field and hydrodynamic forces acting on the hull are discussed based on the computed results. Finally, the propeller effect is implemented behind the wigley hull using the body-force concept by the quasi-steady infinite bladed Blade Element Theory and a propulsion characteristic is observed. The transformed computation code in inertial coordinate is found to be much easier to simulate the different kinds of maneuvering motions compared to the code in non-inertial system and this paper covers the detailed transformation steps and the discussions on the computation results of different motions.

**Keywords:** Inertial coordinate; flat plate; wigley; uniform flow; pure yaw; circular motion test; body-force; blade element theory

© 2014 Penerbit UTM Press. All rights reserved.

## > 1.0 INTRODUCTION

The advent of computer technology becomes a great tool for ship designing field and Computational Fluid Dynamics (CFD) is one of the branches. CFD method offers an alternative to the traditional build and test design approach, i.e., simulation based design (SBD). As the ship hull form geometry is complex and the fluid flow around the ship is in a very difficult mode to cope with, many approaches might be needed in the design of a ship. It has been conjectured that SBD will offer innovative approaches to design an out-of-box concepts with improved performance.<sup>5</sup>

Consequently, it becomes a must to develop computation code on the other side of experimental works. The purpose of this research, the transformation of the original code into an alternative solution methodology, might be a corner for preceding laboratory. The governing equations, Navier-Stokes Equations in inertial coordinate system, are transformed into the body-fitted grid in the moving coordinate system and the velocity components are defined at earth-fixed coordinate. A single block domain grid is generated around the flat plate and Wigley model. The 12 points Finite Analytic Method (FAM) for space discretization and Euler Implicit Scheme for time discretization are used along with

the PISO algorithm for velocity-pressure coupling.<sup>4</sup> The transformed code is simulated with the Wigley hull up to three degrees of freedom by implementing any desired motion of the ship that will be much easier than that of the computation in non-inertial frame.

At the same time, the transformed code in inertial frame is very convenient for the computation of the ship with the propeller effect. In this research, the propeller grid is not used and the propeller effect is computed by the body-force concept with the infinite bladed Blade Element Theory.<sup>8</sup> The computed body-force components are solved in the source terms of the Navier-Stokes equations and the thrust and torque forces are computed within the RANS code.<sup>8</sup> The concept works well in this case and the methodology can be fully applied in other propulsion computations for further research activities.

## > 2.0 METHOD OF COMPUTATION

### 2.1 Grid Generation

The H-type grid is generated around the zero thickness flat plate as well as the Wigley Hull with the same domain size and number



$$X \dot{1} X_0(t) \dot{Z} x \cos(e(t)) \dot{z} \sin(e(t)) \tag{8}$$

$$Z \dot{1} Z_0(t) \dot{Z} x \sin(e(t)) \dot{z} \cos(e(t)) \tag{9}$$

$$Y \dot{1} Y_0(t) \dot{1} 0 \tag{10}$$

$$t \dot{1} t' \tag{11}$$

Using these relations, the momentum equation (Equation 5) is operated differentially by each term and then transformed from the physical domain to the computational domain in non-orthogonal curvilinear coordinates  $(\xi, \eta, \zeta)$ . A partial transformation is used in which only the independent variables are transformed, leaving the velocity components in physical domain. But, all the velocities and geometrical coefficients in the transformed equations still belong to the moving coordinate. According to the purpose of this computation, the velocity components  $(u, v, w)$  are defined in the absolute inertial earth fixed coordinates  $(X, Y, Z)$  so the velocity components with corresponding geometrical coefficients must be transformed into inertial coordinates. Finally, the momentum equations with the velocity components in inertial coordinates in the moving non-inertial grids are obtained and written in Equation 12 in general form. The terms  $u_G, v_G, w_G$  are the grid velocities  $(\dot{X}, \dot{Y}, \dot{Z})$  which are dependable on translational and rotational moments as a function of time (Equation-17). The corresponding coefficients are shown in Equation 20.

$$g^{11} Z_j \dot{Z} g^{22} Z_i \dot{Z} g^{33} Z_j \dot{Z} A Z_i \dot{Z} B Z_i \dot{Z} C Z_j \dot{Z} D Z_h \dot{Z} S Z \tag{12}$$

$$A \dot{1} \frac{Rn}{J} \frac{f_1}{b_1} (u \dot{1} u_G) \dot{Z} b_2^1 (v \dot{1} v_G) \dot{Z} b_3^1 (w \dot{1} w_G) \dot{1} f^1 \tag{13}$$

$$B \dot{1} \frac{Rn}{J} \frac{f_2}{b_1^2} (u \dot{1} u_G) \dot{Z} b_2^2 (v \dot{1} v_G) \dot{Z} b_3^2 (w \dot{1} w_G) \dot{1} f^2 \tag{14}$$

$$C \dot{1} \frac{Rn}{J} \frac{f_3}{b_1^3} (u \dot{1} u_G) \dot{Z} b_2^3 (v \dot{1} v_G) \dot{Z} b_3^3 (w \dot{1} w_G) \dot{1} f^3 \tag{15}$$

$$D \dot{1} R_n \tag{16}$$

$$u_G \dot{1} \frac{dX_0(t)}{dt} \dot{1} z \frac{de(t)}{dt} \cos(e(t)) \dot{1} x \frac{de(t)}{dt} \sin(e(t)) \tag{17}$$

$$v_G \dot{1} \frac{dY_0(t)}{dt} \dot{1} 0 \tag{18}$$

$$w_G \dot{1} \frac{dZ_0(t)}{dt} \dot{Z} x \frac{de(t)}{dt} \cos(e(t)) \dot{1} z \frac{de(t)}{dt} \sin(e(t)) \tag{19}$$

$$b_l^i \dot{1} Y_{lmn} \frac{\dot{S}X^m}{\dot{S}J^j} \frac{\dot{S}X^n}{\dot{S}J^k} (i, j, k \dot{1} \text{ cyclic}) \tag{20}$$

$$g^{ij} \dot{1} \frac{1}{J^2} b_l^i b_l^j \tag{21}$$

$$J \dot{1} \begin{vmatrix} X_j & X_1 & X_n \\ Y_j & Y_1 & Y_n \\ Z_j & Z_1 & Z_n \end{vmatrix} \tag{22}$$

$$f^i \dot{1} \frac{1}{J} \frac{\dot{S}}{\dot{S}J^j} \dot{1} \dot{1} g^{ij} \dot{1} \tag{23}$$

$$S Z \dot{1} \frac{Rn}{J} \frac{A}{\dot{E}} \frac{\dot{S}p}{\dot{S}J} \dot{Z} b_j^2 \frac{\dot{S}p}{\dot{S}1} \dot{Z} b_j^3 \frac{\dot{S}p}{\dot{S}n} \dot{1} \dot{1} 2 \dot{1} g^{12} Z_j \dot{Z} g^{13} Z_j \dot{Z} g^{23} Z_1 \dot{1} f_b \tag{24}$$

In Equation 24,  $f_b$  is the body force and the body forces will be implemented in this term when the propeller is included.

### 2.3 Computational Outline

The transformed equation (Equation 12) is discretized by the 12-point Finite Analytic method in space and Euler implicit scheme for time along with the PISO algorithm for velocity-pressure coupling. For one time step, sufficient iterations are repeated to get a time-accurate solution. The finite analytic coefficients are updated for retaining the linear nature of the Navier-Stokes equations for each internal iteration. The laminar flow computation is carried out at  $Re = 1000$ . In the case of the grid domain inclined with some angles, all the geometrical coefficients must need to be calculated, updated and transformed back into inertial frame at each time step and the velocity-pressure field satisfying Navier-Stokes equations and continuity equations are obtained.

$$F_{Pressure} \dot{1} \int_s p n_i dS \tag{25}$$

$$F_{shear} \dot{1} \int_s h_{s_{ij}} n_i dS \tag{26}$$

The hydrodynamics force on the body surface is obtained by integration of the normal and tangential stresses over the wetted surface area. The fluid stress tensor is composed of the components due to pressure and viscous stress. The pressure and shear forces are calculated by Equation 25-26. The combination of the axial component of the force, the resistance  $\theta_{s,ij}$  is the shear stress component,  $n_i$  is the unit vector normal to the body surface and  $dS$  is the local surface area element.

### 2.4 Boundary Condition

The boundary condition of the computation is shown in Equation 27-30. In the inertial frame, the velocity components and pressure value in the air field could be almost zero. This condition can make the computation much easier to get a converged solution compared to the computation in-inertial frame.

$$\text{Inlet} \quad : \quad u \dot{1} v \dot{1} w \dot{1} p \dot{1} 0 \tag{27}$$

$$\text{Far field} \quad : \quad \text{gradient}(u, v, w, p) \dot{1} 0 \tag{28}$$

$$\text{Free surface (i.e., } y=0) \quad : \quad v \dot{1} 0 \tag{29}$$

$$\text{On the body surface} \quad : \quad u \dot{1} u_G, v \dot{1} v_G, w \dot{1} w_G \tag{30}$$

## 3.0 COMPUTATION IN MANEUVERING MOTIONS

### 3.1 Computation in Uniform Flow

The flat plate with non-dimensionalized length 1, breadth 0.2 and zero thickness is simulated by the transformed code with the body speed gradually accelerating from 0 to 1 towards the negative X direction and then keeping at steady state with advanced speed,  $u_G \dot{1} 1$ . The computational frictional force of flat plate is checked by the well-known Blasius solution ( $B/L \times 0.01328$ ) and the accelerated conditions checked by the infinite plate theory (Equation 31). Good agreements are observed and shown in Figure 4. Velocity distributions on the Wigley hull are shown in Figure 5.

$$F_{frictional} \dot{1} (2 \cdot 1.182 \cdot \sqrt{t} / \sqrt{Re}) \cdot \frac{B}{L} \tag{31}$$

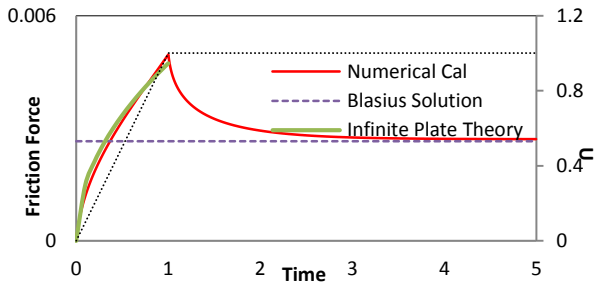


Figure 4 Checking of frictional force on the flat plate

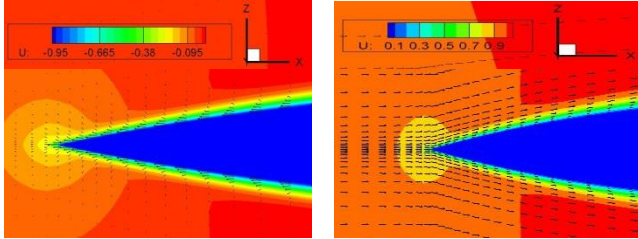


Figure 5 Velocity distributions on the Wigley hull

The pressure force distribution in x-direction is represented by Figure 6. The added mass effect is well observed during the acceleration between t= 0 to 1 and as the steady state is approached the force becomes constant. The shear force distribution on the hull surface is shown in Fig. 7.

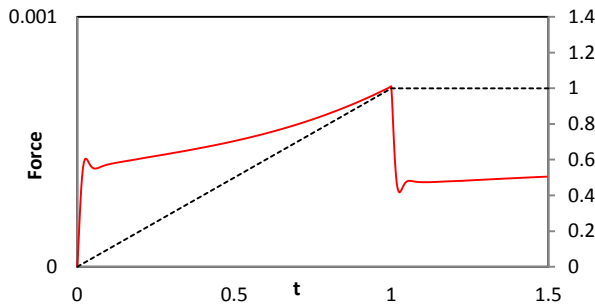


Figure 6 Pressure force distribution on the Wigley hull

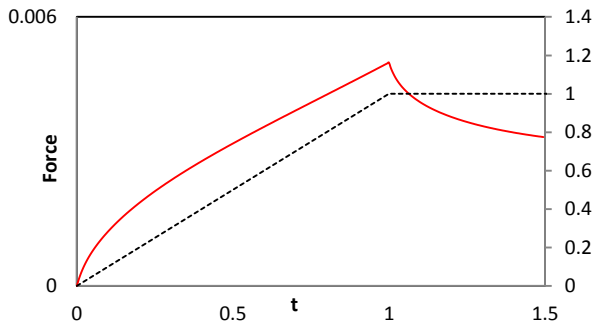


Figure 7 Shear force distribution on the Wigley hull

3.2 Computation in Pure Drift

In nature, the ocean going vessels might probably meet Beam Sea and Oblique Sea that can be a great impact on the hull as well as a

disturbance on the maneuvering behavior. After the Wigley hull has been tested in uniform flow, it then computed with some drift angle to see how the hull surface pressure is distributed.

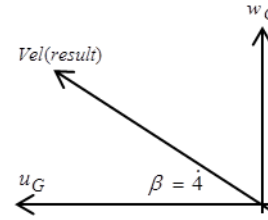


Figure 8 Motion algorithm of pure drift

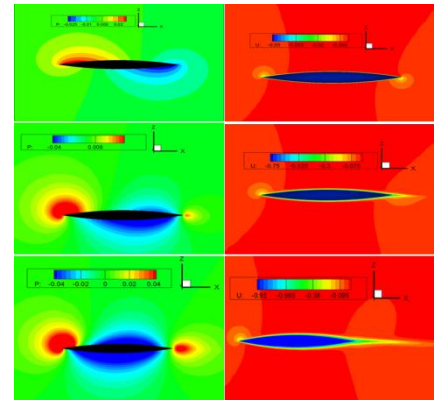


Figure 9 Pressure (left) and velocity (Right) layout in pure drift test.

The ship is given by a motion with drift angle of 4 degree (Figure 8). The resultant velocity is accelerated first and then kept at constant at 1 for the remaining. The grid velocities  $u_G$  and  $w_G$  can be calculated as in Equation 32 where  $V$  is drift angle and implemented into the motion program of the code. The pressure field and the velocity layout along the hull are shown in Figure 9.

$$\begin{aligned} u_G &= 1 \cdot \text{Vel(result)} \cdot \cos V \\ w_G &= 1 \cdot \text{Vel(result)} \cdot \sin V \end{aligned} \tag{32}$$

3.3 Computation in Rotational Motion

When the ship has lateral movement, there might be vorticity generated along the hull and the pressure will be created in high difference. In the PMM test like pure yaw, there will be similar phenomenon so that this is simply tested rotationally as any movement of the ship can easily be carried out in frame computation code. The ship is fixed at the center point in  $(x, z)$  plane at  $(0.5, 0)$  and simply given the motion as in Equation 33 with the angular acceleration  $\omega$  with the time  $t$ . The vorticity generated along the hull while rotating is investigated by Equation 34 and shown in figure 10.

$$e(t) = \frac{1}{2} \omega t^2 \tag{33}$$

$$\begin{aligned} k_x &= \frac{\dot{S}_w}{\dot{S}_Y} - \frac{\dot{S}_v}{\dot{S}_Z} \\ k_y &= \frac{\dot{S}_u}{\dot{S}_Z} - \frac{\dot{S}_w}{\dot{S}_X} \\ k_z &= \frac{\dot{S}_v}{\dot{S}_X} - \frac{\dot{S}_u}{\dot{S}_Y} \end{aligned} \tag{34}$$

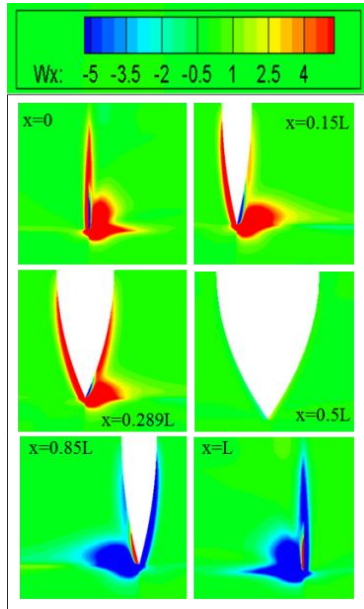


Figure 10 Vorticity distributions along the hull

### 3.4 Computation in Pure Yaw

In the steady movement with  $w_G$ , the hull is given the sway velocity  $w_G$ . The sway distance is a sinusoidal sine with a function of frequency as shown in Equation 35 where  $A$  is the amplitude of the motion,  $k$  is the frequency,  $t$  is the time. In this case, amplitude is taken as 0.05; frequency 2.094 with the period ( $T$ ) of 3 nondimensionally. The sway velocity is the differentiation of the sway distance with respect to time and shown in Equation 36. The value of  $w_G$  is imposed by zero as there is no movement in  $y$ -direction. Additional to sway motion, the yaw angle and the corresponding yaw rate are imposed as in Equation 38 and Equation 39.

$$Z_0(t) = A \sin(kt) \tag{35}$$

$$w_G = \dot{Z}_0(t) = Ak \cos(kt) \tag{36}$$

$$k = 2\pi d/T \tag{37}$$

$$e(t) = \tan^{-1} \frac{w_G}{u_G} = \frac{w_G}{u_G} = \frac{Ak \cos(kt)}{u_G} \tag{38}$$

$$e(t) = \frac{\dot{Z}_0(t)}{u_G} = \frac{Ak^2 \sin(kt)}{u_G} \tag{39}$$

For the yaw rotation, the referenced point is taken at the center of gravity of the plate ( $0.5, 0$ ) in  $(x, z)$  plane. Centered at this point, the ship rotated in a sinusoidal cosine with

function of frequency (Equation 38). The sway and yaw movements are ninety degree phase different. The computation for this case is carried out at zero drift angles. To get rid of the non-uniform disturbance, the simulation is carried out up to three periods of motion. The pressure distribution and the shear force distribution over a cycle of motion are shown in Figure 11. The pressure contours on the hull surface in four quarters of period is shown in Figure 12. The vorticity distributions along the hull from the bow to the stern could be well observed in Figure 13. Each figure represents a quarterly layout in one period of pure yaw movement.

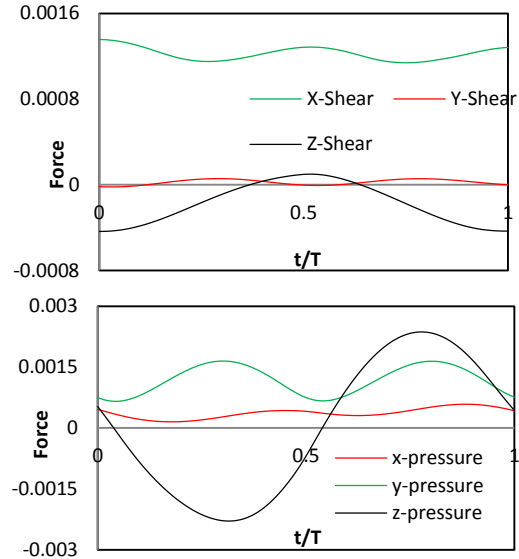


Figure 11 Shear and pressure force distributions on the hull

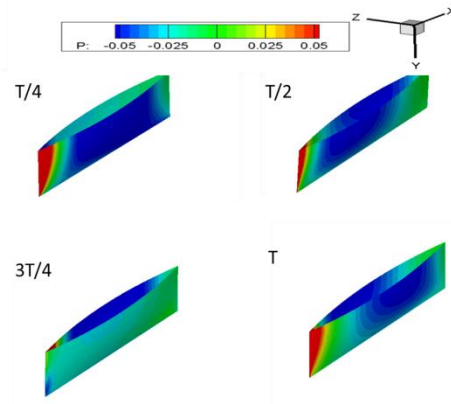


Figure 12 Pressure contours on hull surface



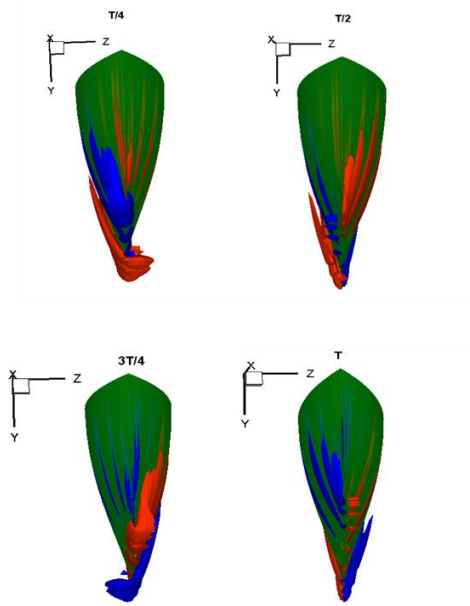


Figure 13 Vorticity distributions on the hull

3.5 Computation in Circular Motion Test

Circular Motion Test (CMT) is an important test in maneuvering field to check the ability of the rudder. This could be easily simulated in inertial frame compared to the non-inertial computation that is one of the reasons the code has been transformed. In this study, CMTs carried out for checking the hydrodynamics forces along the hull and the scope capability of the new computation code. The motion algorithm is shown in Figure 14 with the variables definitions (Equation 40-43) where the translating velocity is  $V_{trans}$ .

$$k = 1 \left| \frac{de(t)}{dt} \right| = 1 \frac{2d}{T} \tag{40}$$

$$V_{trans} = 1 \cdot K \cdot r \tag{41}$$

$$a = 1 \cdot K \cdot Vel \tag{42}$$

$$e(t) = 1 \cdot kt \tag{43}$$

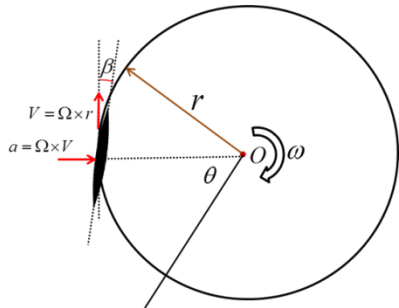


Figure 14 Motion algorithms for circular motion test

The whole domain with the ship to move in the circular path centered at O. In this study, the center of rotation is taken as reference at (0.5, 3) (x, z) plane with the turning radius in inertial frame. The rate of rotation or frequency (Equation 40)

is kept at constant at 0.2. In order to achieve the circular motion with the centripetal force towards the center O, some drift angle  $\beta$  is imposed by 4 degree to the inside of the circle. The simulation is carried out for two cycles of motion and the surge force (x-direction) and sway force (z-direction) on the ship hull in noninertial coordinate is shown in Figure 15.

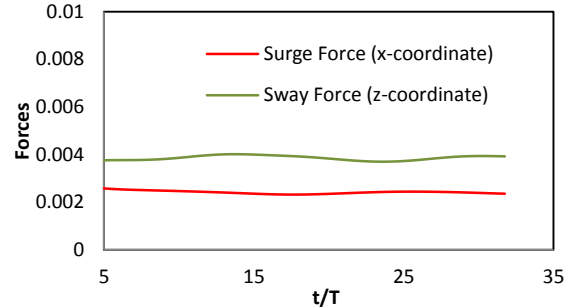


Figure 15 Hydrodynamics forces on the hull in CMT

4.0 COMPUTATION WITH PROPELLER BODY FORCE

The grid generated without propeller grid inside the domain and the propeller effects implemented by the body force concept. The MAU five-bladed propeller which is right handed with a boss ratio of 0.2 is used. The non-dimensional propeller radius 0.4 with a constant pitch 2.062 is placed behind the ship at  $x/L = 11.021$  centered at (0.08594, 0) (y, z) plane. The ship is moving with  $U_G = 11$  steadily and the velocity components in the domain grid at propeller section are transferred to the polar coordinate of the propeller plane which had 51 grids radially with 13 sections tangentially (Figure 16) and, the number of grids well enough to compute the body force by the slender theory as shown in Figure 17.

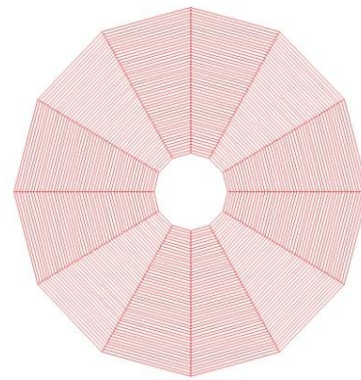


Figure 16 Grids on virtual propeller plane

$$V_R = 1 \sqrt{u^2 + (2chr + v_e)^2} \tag{44}$$

$$V_i = 1 \arctan\left(\frac{u}{2chr + v_e}\right) \tag{45}$$

$$C_l = 1 \cdot 2ck \sin(U \cdot Z \cdot U_{g1}) \tag{46}$$

$$k = 1.07 \cdot 1.05 \cdot \frac{C_{0.7R}}{R} \cdot \frac{N}{O} \cdot 0.375 \cdot \frac{C_{0.7R}}{R} \cdot \frac{N}{O}^2 \tag{47}$$

The computation procedure is as shown in Equation 44. When the propeller is rotating clockwise with tangential velocity  $v_\theta$ , the relative velocity of the fluid anticlockwise with velocity  $v_{rel}$  where  $n$  is the number of revolution. So the resultant velocity with induced velocity effect is computed by Equation 44 and the corresponding hydrodynamic pitch angle  $\alpha$  is computed by Equation 45. The lift coefficient  $C_L$  is based on the zero lift line (dashed line in Figure 17) with  $k$ , a correction for the finite width of the propeller blade, and angle of attack  $(\alpha - \alpha_{go})$  and computed as in Equation 46 and drag coefficient  $C_D$  is assumed as 0.01.

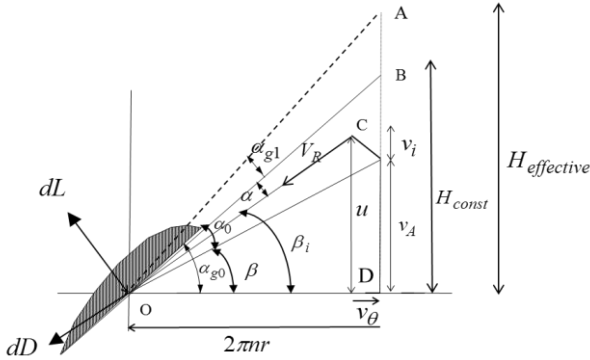


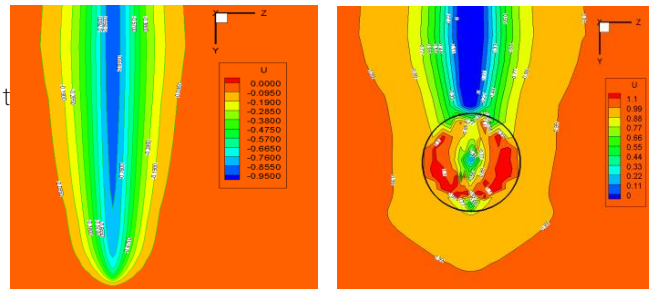
Figure 17 Concept of blade element theory

The thrust and torque forces are computed by Equation 48 and the corresponding forces are calculated by Equation 49 which are transmitted back into the main domain grids and implemented into the source terms of Navier-Stokes equation (Equation 24).

$$\begin{aligned} dL &= 0.5 * C_L * f * V_R^2 * c * dr \\ dD &= 0.5 * C_D * f * V_R^2 * c * dr \\ dT &= dL * \cos \alpha_i \\ dQ &= dL * \sin \alpha_i * \dot{z} * dD * \cos \alpha_i * r \end{aligned} \quad (48)$$

$$\begin{aligned} F_{bx} &= \int \frac{dT}{8x} * \frac{N}{2d} * f * dr \\ F_{be} &= \int \frac{dQ}{8x} * \frac{N}{2d} * f^2 * dr \end{aligned} \quad (49)$$

In nomenclature,  $c$  is the chord length at each radius which is imported from the propeller chord length data files, the radial increment,  $N$  is the number of blades,  $f$  is the non-dimensional density ( $=1$ ) and  $\delta x$  is the grid spacing respectively. The velocity distribution on the propeller plane is shown in Figure 18 and the axial velocity is seen to be higher on the right side due to the effect of right-handed propeller and flow field of ship. The cross-flow vector on the propellers as in Figure 19. The pressure jump on the propeller plane would be well observed in Figure 20. The propellers given the number of rotation based on the ship advanced coefficient and the result of the quarter and thrust coefficient is presented in Figure 21.



(a) Without Propeller (b) With Propeller

Figure 18 Axial velocity contours at x/L=1.021

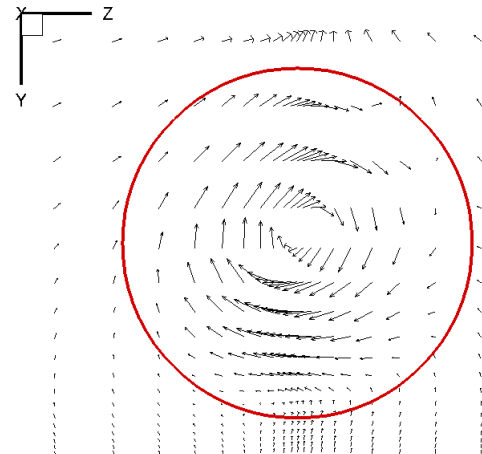


Figure 19 Cross-flow vectors on the propeller plane at x/L=1.021

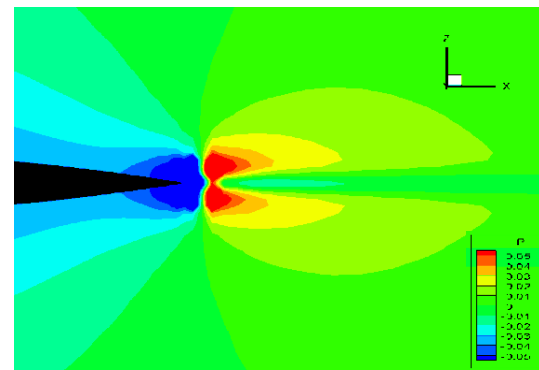


Figure 20 Pressure jump at the propeller plane

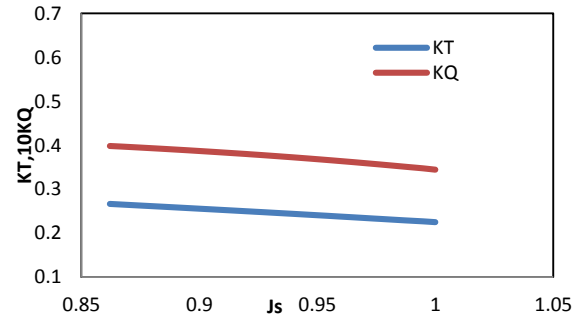


Figure 21 Thrust and torque coefficient with respect to  $J_s$

## › 5.0 CONCLUSION

In conclusion, the previous version of the computation code which is based on non-inertial reference frame is transformed successfully into the one in inertial frame. It is obvious that specification of boundary conditions in the new code is comparatively easier and several ship motion tests can be computed well. The new code is firstly simulated using the flat plate and the results are validated with the hydrodynamics theory as well as with the results in non-inertial frame and well agreements are observed. Using the wigley model, important maneuvering motions like pure yaw and circular motion test can be simulated well and hydrodynamics behavior around the hull is well observed. Moreover, the propeller effect by the body-force concept can be implemented behind the ship and the propulsion quantities are computed and observed well. The concept of the transformation technique, the advantage of the computation in inertial frame and the introducing of the new propeller body-force concept that are all covered in this paper is the important step which will strongly support the future research projects.

## Acknowledgement

We give our special thanks to all of the members of the third laboratory, Department of Naval Architecture and Ocean Engineering, Osaka University who have involved in this research project.

## References

- [1] Schlichting, H. 1979. *Boundary-Layer Theory Seventh Edition*. 135: 140.
- [2] Van-Dyke, M. 1982. *An Album of Fluid Motion*. 18: 22.
- [3] Stern, F., Paterson, E. G., Tahara, Y. 1996. *CFDSHIP-IOWA: Computational Fluid Dynamics Method for Surface-Ship Boundary Layers, Wakes and Wave Fields*. IHR Report 381. 2: 33.
- [4] Xing, T., Carrica, P., Stern, F. 2008. *Computational Towing Tank Procedures for Single Run Curves of Resistance and Propulsion*. 130(1): 1-6.
- [5] Ueno, M., Yoshimura, Y., Tsukada, Y., Miyazaki, H. 2009. *Circular Motion Tests and Uncertainty Analysis for ship maneuverability*. 1: 3.
- [6] Brogli, R., Muscari, R., Mascio, A. D. 2006. *Numerical Analysis of Blockage Effects in PMM Tests. The 26<sup>th</sup> Symposium on Naval Hydrodynamics*. 27: 28.
- [7] Cura-Hochbaum, A. 2006. *Virtual PMM Test for Manoeuvring Prediction. The 26<sup>th</sup> Symposium on Naval Hydrodynamics*. 31: 40.
- [8] Kuroda, K. 2012. *Graduation Thesis of Department of naval Architecture and Ocean Engineering, Osaka*. 8: 11.